scientific reports

Check for updates

OPEN

Demonstration of time-resolved Fe K-edge XANES with a self-seeded X-ray free-electron laser at PAL-XFEL

Rory Ma[1,2,4], Yujin Kim[1,4], Inhyuk Nam[3], Gyujin Kim[1], Minseok Kim[1], Gisu Park[1] & Jae Hyuk Lee[1,2]✉

We demonstrate, for the first time, time-resolved X-ray absorption near-edge structure (XANES) spectroscopy at the Fe K-edge using a self-seeded X-ray free-electron laser (XFEL) beam at the FXL endstation in Pohang Accelerator Laboratory X-ray Free-Electron Laser (PAL-XFEL). Focusing on the application of self-seeded XFEL for time-resolved XANES, we show advantages in photon flux, measurement speed, and signal-to-noise ratio (S/N). Using the high-stability, narrow-bandwidth self-seeded mode, we achieved an incident X-ray bandwidth of approximately 0.71 eV and improved spectral purity compared to conventional self-amplified spontaneous emission (SASE) operation. A 50 mM aqueous solution of iron(II) tris(1,10-phenanthroline) dichloride was photo-excited by a 400 nm femtosecond laser, and ultrafast electronic dynamics were probed by synchronized XFEL pulses. The enhanced spectral purity and energy stability enabled clear detection of transient features obscured by SASE pulse bandwidth and energy jitter. The results highlight the clear benefits of the self-seeded XFEL source, showing a 25% improvement in signal-to-noise ratios compared to the SASE with double crystal monochromator (DCM) mode, particularly for time-resolved XANES experiments. This work lays the foundation for advanced exploration of chemical and biological dynamics with improved spectral accuracy in complex environments.

Keywords Time-resolved XANES, Self-seeding, X-ray free electron laser, Ultrafast X-ray absorption spectroscopy, Transition metal complexes, Time-resolved spectroscopy

X-ray free-electron lasers (XFELs) have heralded a new era in ultrafast science, providing intense, femtosecond-duration X-ray pulses with exceptionally high spatial coherence and unprecedented brightness[1–3]. These properties have expanded the frontiers of research in chemistry, physics, biology, and materials science, facilitating unprecedented time-resolved studies of structural and electronic dynamics in diverse systems ranging from biological macromolecules to quantum materials and catalytic intermediates[4,5]. X-ray absorption spectroscopy (XAS) at XFEL facilities provides a unique, element-specific probe of ultrafast electronic and geometric structure changes, enabling the direct observation of photo-induced processes and charge transfer reactions with femtosecond time resolution[6–10].

Continuous advancements in time-resolved X-ray spectroscopy (TR-XAS) at XFELs have been persistently driven by the pursuit of enhanced experimental capabilities. Key goals in the community have included improving data acquisition speed, minimizing sample consumption, and refining spectral resolution to capture complex dynamics with greater fidelity.

The standard operational mode for XFEL facilities is SASE mode[11,12], which, despite delivering high power, is rooted in stochastic amplification. This process leads to poor temporal coherence, manifested as a chaotic and broad spectrum with a bandwidth of ~ 0.1–0.5% and significant shot-to-shot fluctuations[13,14]. This inherent spectral and energy instability fundamentally hinders the acquisition of high energy resolution spectrum, where precise control over the incident X-ray energy is critical for resolving subtle features. A conventional solution

[1]Pohang Accelerator Laboratory, Pohang University of Science and Technology, Pohang 37673, South Korea. [2]Photon Science Center, Pohang University of Science and Technology, Pohang 37673, South Korea. [3]Department of Physics, Ulsan National Institute of Science and Technology, Ulsan 44919, South Korea. [4]These authors contributed equally: Rory Ma and Yujin Kim ✉email: jaehyuk.lee@postech.ac.kr

has been using a downstream double-crystal monochromator (DCM) to narrow the bandwidth and improve spectral resolution[15]. However, this approach severely reduces the usable photon flux, limiting the achievable signal-to-noise ratios (S/N) and increasing data acquisition times for dilute or weakly absorbing samples.

Among these developments, the integration of large-bandwidth self-amplified spontaneous emission (SASE) pulses with dispersive detection schemes represents a significant breakthrough[6, 16, 17]. The primary advantage of this approach lies in its ability to rapidly acquire full X-ray absorption near-edge structure (XANES) spectrum, often in a single shot, without the need for photon energy scanning. This capability dramatically enhances data collection speed and minimizes the consumption of valuable samples, opening new frontiers for investigating ultrafast dynamics and radiation-sensitive systems.

Despite these clear advantages for rapid, full-spectrum acquisition, this broadband approach faces inherent technical challenges. These are primarily constrained by the limited intrinsic energy resolution of the inline spectrometers and the significant shot-to-shot spectral fluctuations typical of stochastic SASE pulses. Consequently, sophisticated post-processing is often required to yield high-quality data.

To complement the capabilities of broadband methods and address the rigorous demands for higher spectral precision, we have focused on increasement of the signal level via developing techniques based on self-seeded FEL operation. In contrast to SASE, the self-seeding process selectively amplifies a narrow-bandwidth seed pulse. This fundamental difference concentrates the entire photon flux into a very narrow energy window, generating highly monochromatic X-ray pulses with superior energy resolution and spectral purity.

As a result, these self-seeded pulses are uniquely advantageous for experiments targeting weakly absorbing samples, dilute solutions, or photo-hungry techniques such as high-energy-resolution fluorescence detection (HERFD) and resonant inelastic X-ray scattering (RIXS). These sophisticated applications are critically dependent on both high spectral resolution and intense photon flux. This positions the self-seeded approach as a powerful and complementary tool to the broadband SASE methods, collectively broadening the scientific scope of XFEL-based research.

Self-seeding schemes have been developed and implemented at the Pohang Accelerator Laboratory X-ray Free-Electron Laser (PAL-XFEL)[18,19]. This method utilizes a single-crystal diamond monochromator to spectrally filter the initial SASE beam. This carves out a spectrally pure seed pulse, which is then amplified in a downstream undulator section. The resulting self-seeded FEL pulse exhibits a significantly narrow bandwidth and much greater peak brightness than conventional SASE[18–21]. Consequently, self-seeded operation is particularly well-suited for XAS and XANES experiments requiring high resolution and rigorous reproducibility[22].

The present study specifically benchmarks the self-seeded mode against traditional broadband SASE operation, highlighting key methodological differences and their impact on energy resolution and measurement speed. Despite these advances, demonstrated studies of time-resolved XANES using self-seeded hard XFEL pulses have remained scarce, constrained by technical complexity and the relatively recent development of self-seeded FEL worldwide. The PAL-XFEL has recently commissioned high-brightness hard X-ray self-seeding, creating an optimal platform to explore the capabilities of narrow-bandwidth XFEL pulses in ultrafast spectroscopy—including transient electronic structure characterization in transition metal complexes in solution or solid phases[18,19,23].

In this work, we present a systematic and quantitative evaluation of time-resolved XANES performance using a hard X-ray self-seeded FEL at PAL-XFEL, addressing both the opportunities and the remaining challenges of this advanced platform. By directly and rigorously benchmarking self-seeded and SASE operation, we evaluate not only the gains in spectral purity, energy resolution, and reproducibility, but also critically examine practical issues such as detector optimization, intensity fluctuations, and residual SASE background. A key focus is on assessing the achievable improvements in S/N and exploring the practical potential for future high-resolution experiments.

Using Fe-centered coordination complexes as a model, we demonstrate the clear advantages of self-seeded FEL pulses for observing ultrafast transient electronic structures. These results define a new benchmark for high-resolution, time-resolved XAS at XFELs, and serve as a practical foundation for the extension of ultrafast X-ray spectroscopy to challenging and weakly absorbing systems in chemical, biological, and material sciences. Our discussion also outlines the technical limitations encountered and suggests directions for future optimization, advancing both the understanding and broader applicability of self-seeded FELs for the scientific community.

Results

Photon energy control system for self-seeded FEL operation

The physical mechanism for self-seeded FEL implemented at PAL-XFEL is schematically depicted in Fig. 1. In this scheme, SASE radiation generated in the upstream undulators is filtered by a single-crystal diamond monochromator via forward Bragg diffraction. In this study, a self-seeded beam is generated with [202] orientation of diamond crystal. This monochromator acts as a narrow-bandwidth spectral filter, producing a highly monochromatic seed pulse that is temporally separated from the residual SASE. The seed pulse is then injected into downstream undulator segments where it is amplified, resulting in a self-seeded FEL output with significantly enhanced spectral coherence and energy stability compared to conventional SASE FEL operation[19,20].

At PAL-XFEL, the photon energy control system is a vital component supporting time-resolved XANES experiments with a self-seeded FEL. The system achieves enhanced spectral purity and improved energy stability necessary for resolving transient electronic structural dynamics in solution samples[24]. It controls the electron bunch energy and the angle of diamond monochromator in the seeding section of undulator. The electron bunch energy is carefully tuned to align the SASE FEL with the desired photon energy, serving as an efficient seed for the downstream undulator amplification. Alongside this, the angle of the diamond monochromator crystal is precisely adjusted to maximize the intensity and spectral sharpness of the self-seeded beam. These optimizations

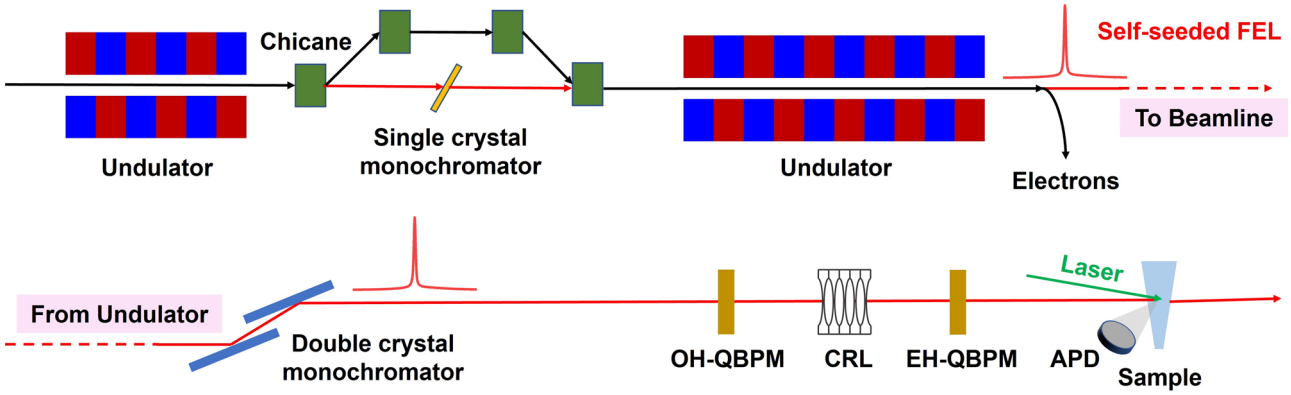

Fig. 1. Schematic illustration of the self-seeded FEL mechanism at PAL-XFEL. FEL from SASE is passed through a single-crystal diamond monochromator. Using forward Bragg diffraction, the monochromator filters the broad-bandwidth SASE pulse to generate a narrow-bandwidth seed pulse. While passing through the rest undulators, the seed pulse is then amplified to produce a highly monochromatic, self-seeded FEL pulse with enhanced spectral resolution. The residual SASE background is further suppressed by DCM. The OH-QBPM provides feedback control, while the EH-QBPM is used for normalization of incident intensity (I_0). A compound refractive lens (CRL) focuses the X-ray beam onto the sample position, where the optical laser and X-ray pulses are spatially overlapped. X-ray absorption is measured using APD detector.

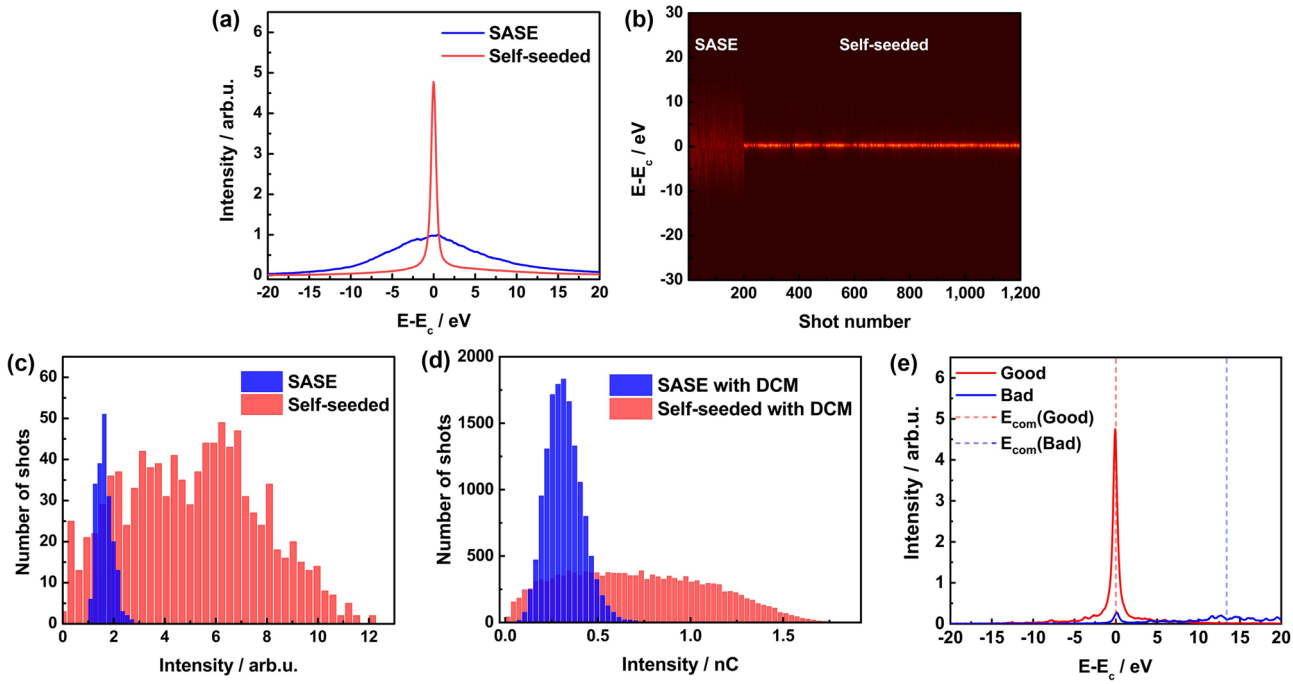

Fig. 2. Comparison of SASE and Self-seeded FEL spectral properties. **a** The average spectral intensities of SASE (blue) and self-seeded (red) FELs at the Fe K-edge, **b** Shot-to-shot spectra of 200 consecutive pulses for SASE (#1–#200) and 1,000 consecutive pulses for self-seeded FEL (#201–#1,200), **c** Histograms showing the distribution of integrated intensities for both SASE (blue) and self-seeded (red) FEL pulses within a 1 eV bandwidth, **d** Histograms showing the distribution of EH-QBPM intensities for both SASE with DCM (blue) and self-seeded with DCM (red) at 7.125 keV and **e** Representative good(red) and bad self-seeded(blue) FEL single shots and their corresponding E_{com}-E_c, (-0.004 eV for good shot and 13.399 eV for bad shot), respectively.

result in a typical energy resolution around 0.71 eV (FWHM) near the Fe K-edge, significantly narrower than SASE mode bandwidths which exceed 10 eV (Fig. 2a). We clarify that the FWHM bandwidth of the self-seeded FEL at ~ 0.71 eV represents only the incident pulse spectral width, and the intrinsic energy resolution of the XANES experiment further depends on the monochromator and how to detect the signal. As such, the measured XANES spectral features can be broadened and distorted by these factors.

The photon energy control system at PAL-XFEL is fundamental in enabling the detection of subtle transient spectral features with improved S/N compared to conventional SASE operation. Furthermore, the integration of DCM effectively filters residual SASE background, enhancing spectral purity. Collectively, this system provides a robust platform for advancing ultrafast XANES studies of transition metal complexes and related chemical dynamics under realistic solution conditions at PAL-XFEL.

The incident X-ray spectrum was recorded downstream of the DCM using single-shot spectrometers tailored to different operational modes. For measurements centered at E_c = 7.1 keV, a Si(220) curved crystal with a 100 mm radius of curvature was coupled with an Andor ZYLA5.5X-FO detector (2560 × 2160 pixels, 6.5 × 6.5 μm^2 pixel size), providing a spectral resolution near 0.31 eV enabling coverage of the broad spectral range of the entire SASE profile[25]. As shown in Fig. 2a, the self-seeded beam exhibited a relatively narrow bandwidth averaging 0.71 eV (FWHM) with a pulse energy around 0.9 mJ in the Fe K-edge region, whereas the SASE beam showed a substantially broader bandwidth of about 12.5 eV and a higher pulse energy of approximately 1.8 mJ. Despite delivering lower overall pulse energy, the self-seeded beam produced a much sharper and more intense spectral peak than the SASE mode, demonstrating the advantage of concentrating photon flux within a narrow energy bandwidth to enhance spectral brightness and coherence. The peak intensity of self-seeded beam is 4.8 times higher than that of SASE beam.

Figure 2b and c show the measured spectra from 200 consecutive shots of SASE FEL and 1,000 consecutive shots of self-seeded FEL, along with their corresponding histograms. We compared the shot-to-shot fluctuation of center energy between a SASE and a self-seeded FEL. The fluctuation for the self-seeded beam was calculated based on the peak position of the spectrum, a suitable metric given its stable, narrow-bandwidth spectrum. To preclude the influence of anomalous shots, shots with a peak position deviating more than 3 eV from the average were excluded from the self-seeded data set. In contrast, the fluctuation of the SASE beam was determined from the center of mass of the intensity distribution over a 60 eV energy range to account for its inherent multi-spike and broad spectral profile. The analysis revealed a significant difference in stability, with the self-seeded beam showing a fluctuation of only 0.1057 eV, which is more stable than that of 2.66 eV fluctuation observed for the SASE beam. This result clearly demonstrates the substantial improvement in spectral stability achieved by self-seeding.

As shown in Fig. 2c, the integrated intensity over a 1 eV bandwidth followed a Gaussian distribution. The pulse-to-pulse root mean square (RMS) jitter of x-ray intensity was measured to be 18.5% for the SASE beam, 28.7% for the SASE beam after DCM and 50% for the self-seeded beam, as calculated from the fluctuations in the integrated intensity over a 1 eV bandwidth. While the self-seeded FEL exhibited significant intensity fluctuations, normalization to the well-controlled incident beam intensity allowed us to successfully overcome this challenge and achieve reliable measurements. As shown in Fig. 2a, the self-seeded beam is characterized by a sharply defined, narrow-bandwidth peak with an average energy resolution of 0.71 eV. This contrasts sharply with the SASE beam's stochastic, broad spectral distribution, which results in a much larger shot-to-shot energy jitter. The self-seeded beam's spectral properties enable the clear resolution of fine spectral features that would otherwise be obscured by the broad bandwidth and energy jitter inherent to SASE pulses. The higher intensity fluctuations observed in the self-seeded mode (50% RMS jitter) are a characteristic of the self-seeding amplification process and do not diminish its primary benefit for high-resolution XAS, that is the concentration of photon flux into a highly stable, narrow energy bandwidth. The peak intensity of the self-seeded beam is 4.8 times greater than that of the SASE beam, and its integrated intensity within a 1 eV window is 3.2 times higher.

Figure 2d presents the intensity distribution of individual FEL shots as measured by the experimental hutch quadrant beam position monitors (EH-QBPM), which are positioned just downstream of the DCM. This analysis is based on a total of 14,580 shots collected under both SASE and self-seeded operational modes. The application of the DCM enables robust separation and filtering of these pulses, discriminating against high-quality seeded shots from broader, less stable SASE background. Quantitative analysis reveals that for SASE with DCM, the mean integrated intensity 3.19×10^{-10} with an RMS of 30%, while self-seeded with DCM shows the mean integrated intensity of 7.14×10^{-10} with an RMS of 54%.

Figure 2e shows the spectra of a good and a bad self-seeded FEL single shot. The spectrum of a good shot is the ideal result of a successful self-seeding process. It is dominated by a single, sharply defined peak with an extremely narrow bandwidth. This is a direct consequence of the monochromator filtering a specific wavelength from the initial SASE pulse, which then acts as a seed to amplify a highly monochromatic FEL pulse in the second undulator section. For this good shot, the center of mass energy (E_{com}) of the spectrum is perfectly aligned with the target photon energy, E_c. In stark contrast, the spectrum of a bad shot reveals a failure in the self-seeding mechanism. The spectrum shows a mixture of a small, weak seeded peak superimposed on a broad SASE background. This signifies that the seeded pulse was not sufficiently strong to dominate the amplification process in the second undulator, allowing the broad-bandwidth SASE component to persist. The most significant feature of the bad shot is that its E_{com} is substantially shifted away from E_c. This large energy offset makes the shot unsuitable for energy scan experiments, as it would introduce noise and error into the data while these poor-quality shots can be filtered out using a DCM.

Beam position feedback and beam energy control system

A DCM employs two Si(111) crystals to precisely select and filter the desired X-ray energy using the Bragg condition, with the crystal angle being finely tuned during energy scans. However, even minor misalignments of the DCM which result either from stage drift or incremental changes in the Bragg angle during energy scans can induce substantial shifts in the downstream X-ray beam position. This effect is amplified by the long propagation distance between the DCM and the sample position (approximately 30 m), causing the beam at the sample to deviate by several millimeters per microradian of angular error. Such beam trajectory instability directly impacts the spatial overlap between the X-ray and optical laser beams at the interaction region, leading to reduced

transient signals in pump-probe measurements. For quantitative time-resolved experiments, consistent beam positioning must be ensured across the entire energy range to maintain reliable and uniform excitation and measurement conditions.

To address these challenges, we implemented a real-time positional feedback system utilizing QBPMs downstream of the DCM in the optical hutch (OH-QBPM). QBPM incorporates a thin foil scattering target (e.g., silicon nitride or chemical vapor deposition diamond) and a set of four large-area photodiodes arranged to capture the backscattered X-ray signal. Differential signals from the upper versus lower and left versus right photodiodes yield quantitative measurements of the vertical (y-axis) and horizontal (x-axis) beam positions, respectively. The system continuously computes these positional signals and relays them to a closed-loop controller that dynamically corrects for beam displacements by adjusting the DCM pitch and roll motors.

Real-time QBPM readouts are processed using a proportional-integral-derivative (PID) algorithm to minimize the deviation from a desired beam position. The controller's output commands precise adjustments to the roll and pitch motors of the DCM, which in turn realign the beam path. This process ensures the beam position at the sample is stabilized throughout energy scans. Performance benchmarking showed that the feedback maintained beam alignment within the spatial overlap tolerance even during extended energy scans or under moderate environmental perturbations, thus ensuring reliable X-ray/laser coincidence for pump–probe experiments.

Critically, Fig. 3 demonstrates that, under self-seeded XFEL operation, the photon energy control system, in combination with the beam position feedback system, enabled excellent stability of the Incident X-ray intensity

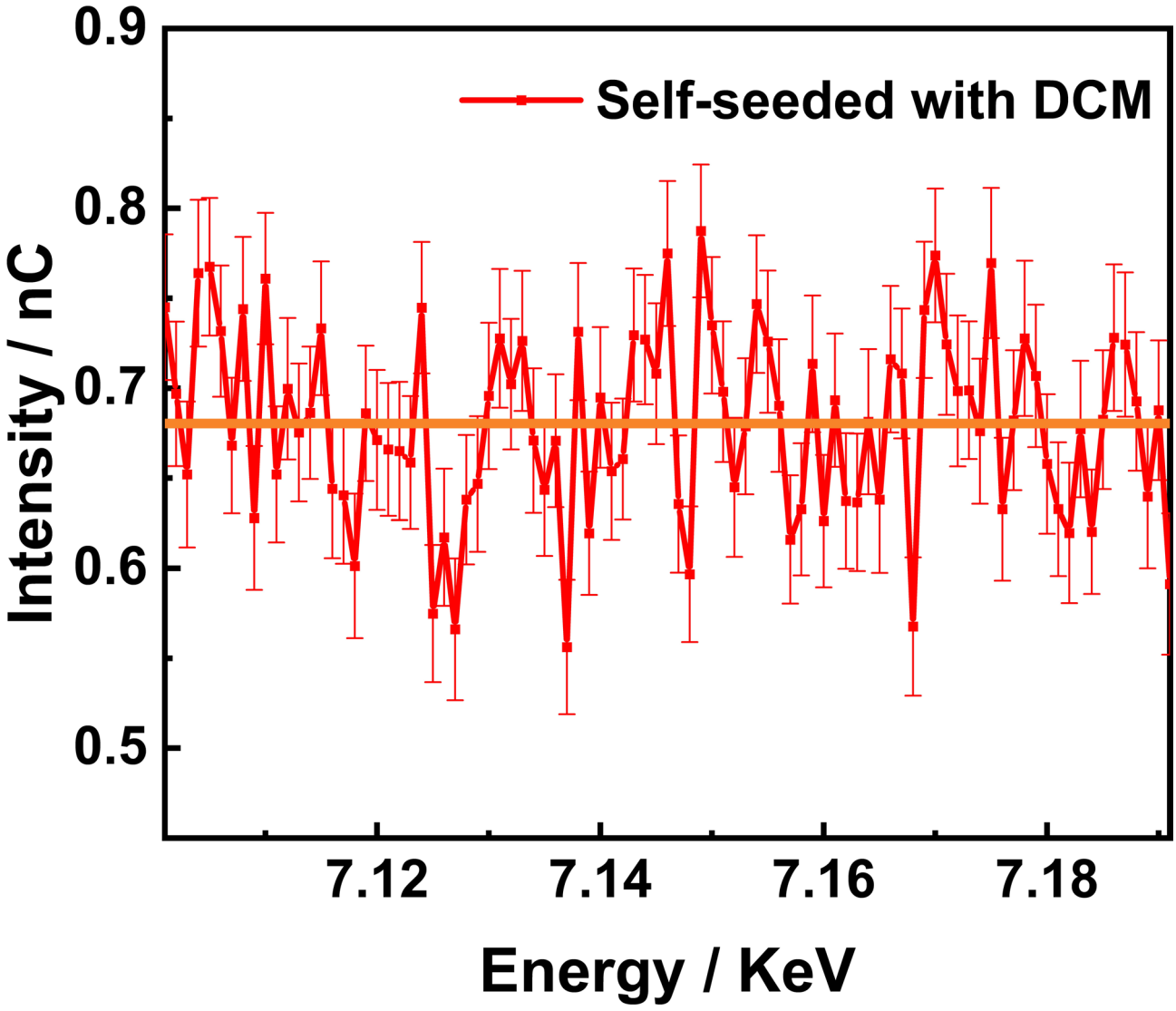

Fig. 3. Monitoring I_0 during a photon energy scan. Data was collected at the Fe K-edge using a self-seeded FEL and a DCM configuration. Each energy point represents an average of 180 shots. The incident intensity was monitored with QBPM in the experimental hutch. The orange line represents the mean value of the I_0 intensity. The error bars represent the standard error of the mean (SEM), calculated from repeated measurements at each energy point ($N = 180$).

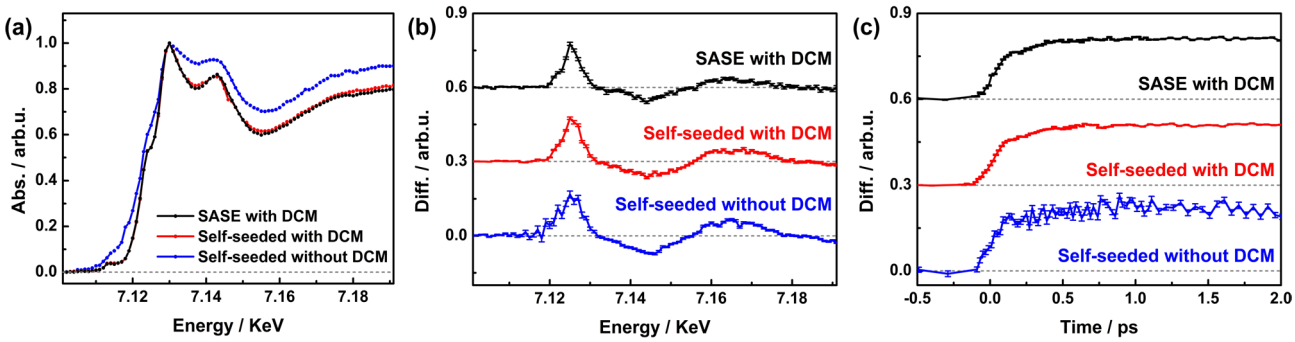

Fig. 4. XANES results using the SASE FEL with DCM (black), self-seeded FEL with DCM (red), and self-seeded FEL without DCM (blue): **a** Normalized static absorption spectra, **b** Differential absorption spectra measured at 50 ps after 400 nm excitation and **c** Time-resolved delay scans of the relative absorption change at 7.125 keV. The error bars indicate the standard error of the mean (SEM), computed from repeated measurements for each point.

(I_0) intensity as measured by the QBPM in the experimental hutch. During TR-XANES measurements, the Bragg angle of the diamond crystal, the SASE energy, and the Bragg angle of the DCM were synchronized and moved simultaneously to maintain a constant incident beam flux at various self-seeded FEL energy. As a result, across the full scan range of Fe K-edge photon energies, the relative standard deviation (RSD) of I_0 was maintained at only 7% over 180 consecutive shots at each energy point (mean charge: 0.680 nC). This high level of intensity stability is essential for reliable XAS measurements during energy scans and highlights the robust performance of the implemented control systems.

Time-resolved Fe K-edge XANES measurements

$Fe(phen)_3Cl_2$ was chosen as a model system for the commissioning of TR-XANES experiments with self-seeded FEL. This compound is a well-established subject of study in ultrafast spectroscopy, making it an ideal candidate for evaluating the performance of our pump-probe setup. In its ground state, $Fe(phen)_3Cl_2$ is a low-spin (LS) complex with iron coordinated to six nitrogen atoms in an octahedral geometry. Each of the three phenanthroline ligands contributes two nitrogen atoms to this coordination. When photo-excited by a pump pulse, the complex undergoes a spin crossover to a high-spin (HS) state. This rapid transition from the LS to the HS state provides a clear spectroscopic signature, which is well studied using synchrotron or FEL sources for time-resolved measurements[26–28]. By using this system, we can effectively demonstrate and validate the capabilities of our experimental platform for investigating ultrafast chemical and structural dynamics.

For the XANES measurements, the SASE beam was monochromatized using a Si(111) DCM. The XANES spectra with this monochromatized beam(mono-beam) were compared with those with the self-seeded beam under two conditions, with and without DCM, as shown in Fig. 4. The DCM was also employed with the self-seeded beam to assess the effect of any residual SASE background on the spectra. The static absorption spectra of aqueous $Fe(phen)_3Cl_2$ at Fe K-edge is shown in Fig. 4a which is normalized at the absorption maximum energy. It exhibits sharp and well-resolved spectral features with both the SASE with DCM and the self-seeded beam with DCM, whereas the self-seeded beam without DCM displays broader features and reduced resolution due to residual SASE background. In Fig. 4b, differential X-ray absorption spectra at time delay of 50 ps between 400 nm optical pulses and X-ray probe pulses indicates that the SASE and self-seeded beam with DCM is more advantageous for capturing transient features with high accuracy, whereas the self-seeded beam without DCM fails to resolve the subtle structural details. Figure 4c shows the time evolution of the transient positive peak at 7.125 keV. The markedly larger error bars measured with the self-seeded beam without DCM are primarily attributed to increased broad FEL spectrum from the SASE background as shown in Fig. 2d. This finding quantitatively confirms the necessity of effective monochromator filtering for reliable time-resolved measurements in self-seeded XFEL mode. S/N were derived by evaluating the average signal (absorption or differential absorption) divided by the SEM in regions of interest, allowing quantitative comparison between SASE and self-seeded beam conditions. Although the self-seeded beam with DCM yielded an approximately 25% higher S/N compared to the SASE beam under similar conditions evaluating error bars, this improvement was not fully realized due to the need to increase the digitizer dynamic range to prevent detector saturation at the higher photon flux, which introduced additional electronic noise. Consequently, the S/N comparison presented here should be considered a conservative estimate of the system's potential. Further optimization of the detector dynamic range and data acquisition electronics could reduce electronic noise and better capitalize on the increased photon flux delivered by the self-seeding approach. This enhanced photon flux per eV at the sample is the primary technical advantage underpinning the benefits of self-seeding for TR-XANES, supporting more efficient data collection and improved sensitivity, especially for weakly absorbing or dilute samples.

Collectively, these results demonstrate that the combination of self-seeded XFEL operation and monochromator filtering at PAL-XFEL represents a significant step forward in ultrafast X-ray spectroscopy, particularly for model systems. While these advances enable improvements in spectral resolution, photon flux, and measurement sensitivity for $Fe(phen)_3Cl_2$, further systematic studies with a broader range of samples,

especially those with lower concentration or more complex matrices, will be required to fully evaluate and generalize the platform's capabilities for applications in photocatalysis, materials science, and biochemistry.

Perspectives

While the development of self-seeded XFEL sources at PAL-XFEL represents a significant step forward for ultrafast X-ray spectroscopy, the present work demonstrates these advances mainly with a single well-characterized model system. The results confirm that higher spectral purity and photon flux are valuable for TR-XANES studies of $Fe(phen)_3Cl_2$ and indicate possible future benefits for weak-signal or high-resolution applications such as high-energy-resolution fluorescence detection and resonant inelastic X-ray scattering.

Methods

X-ray source and beamline configuration

XAS experiments were performed at the XSS-FXL beamline of PAL-XFEL. The XFEL was operated in two distinct modes: self-seeded and SASE. For self-seeded operation, experiments were conducted both with and without DCM to evaluate the effect of spectral filtering on beam quality and spectral purity. The use of DCM enabled a narrower bandwidth and significantly improved energy stability, allowing for a detailed comparison between filtered and unfiltered self-seeded pulses. The SASE mode, characterized by a broader bandwidth and significant shot-to-shot energy jitter, served as a baseline for comparison.

Sample delivery

A 50 mM aqueous solution of iron(II) tris(1,10-phenanthroline) dichloride ($Fe(phen)_3Cl_2$) was circulated using magnetic pump through a 150 μm-thick liquid jet. The sample was prepared by dissolving iron(II) chloride tetrahydrate and 1,10-phenanthroline monohydrate in deionized water, followed by stirring and purification to obtain a clear, stable solution suitable for spectroscopic measurements. Continuous flow ensured sample refreshment between pulses, reducing radiation damage and maintaining sample integrity throughout the measurements.

Pump pulses were delivered by a Ti: Sapphire laser system operating at 400 nm wavelength with an approximately 35 fs (FWHM) pulse duration and a 30 Hz repetition rate, synchronized with the XFEL source. The pump beam was focused onto the sample with a measured spot size of about 140×140 μm^2 (FWHM), and the fluence was adjusted to 100 mJ/cm^2 to ensure efficient excitation while minimizing sample damage. The X-ray probe pulses, operated in 60 Hz mode, were focused using a compound refractive lens (CRL) system to achieve a spot size of 38×38 μm^2 at the sample position, enabling high spatial overlap and intensity for time-resolved measurements. Temporal overlap and delay between the optical pump and X-ray probe pulses were controlled using a motorized delay stage with several femtoseconds timing resolution. Spatial overlap at the sample position was monitored and confirmed via imaging on a YAG: Ce scintillator screen.

Beam position stabilization and DCM feedback system

For stable and reproducible time-resolved XANES measurements, a sophisticated feedback control system was implemented for DCM to maintain photon energy stability and beam alignment. QBPMs positioned downstream of the DCM continuously monitored the X-ray beam position by detecting backscattered signals from thin Si_3N_4 foils, providing real-time positional data.

These signals were processed by a PID controller integrated into the experimental physics and industrial control system (EPICS) control system framework. The PID controller actively adjusted the angular positions (roll and pitch) of the two DCM crystals to compensate for slow drifts, thus maintaining beam alignment and spectral purity during scans. The feedback loop operated with a response time of approximately one second, effectively suppressing beam position drift at the sample.

This dynamic correction is critical to preserving stable beam footprint and photon energy consistency, thereby reducing spectral jitter, and enhancing spectral resolution in time-resolved measurements. Users could monitor and adjust PID gain settings via a graphical user interface (GUI), ensuring optimal feedback performance throughout the experiments.

XANES data acquisition

XANES spectra at the Fe K-edge were collected by measuring X-ray absorption using an avalanche photodiode (APD) detector that offered single-shot sensitivity and rapid response. Incident beam intensity (I_0) normalization was performed using QBPM signals to correct for pulse-to-pulse fluctuations, improving signal-to-noise ratio and accuracy.

Additional considerations

Beam focal sizes were characterized by knife-edge scans, and temporal synchronization optimized for maximum signal detection. Direct comparison of self-seeded (with and without DCM) and SASE modes elucidated the impact of monochromator filtering and self-seeded on spectral quality and temporal resolution in time-resolved XANES.

Conclusion

In summary, this study demonstrates the feasibility of time-resolved Fe K-edge XANES measurements using self-seeded technology at PAL-XFEL, as validated with a well-established model system, $Fe(phen)_3Cl_2$. The results confirm that self-seeded operation can provide higher spectral purity and improved flux compared to conventional SASE-based approaches, leading to enhanced spectral resolution and sensitivity for time-resolved

X-ray spectroscopy of this test compound. However, the full advantage of weaker signals or more complex experimental systems was limited by factors such as intensity fluctuation and detector optimization. The comparative analysis revealed both strengths and current practical limitations, confirming that while the self-seeded XFEL's potential for signal-limited and nonlinear spectroscopies is promising, it requires further technical developments. Continued improvement in beam stability, detection electronics, and experimental protocols will be essential for realizing the broader impact of self-seeded XFELs across diverse chemical and material systems. The findings presented here should therefore be regarded as an important foundation for future developments, rather than a definitive solution for all ultrafast X-ray spectroscopy.

Data availability

The datasets generated or analyzed during the current study are available from the corresponding author upon reasonable request.

Received: 4 September 2025; Accepted: 9 December 2025
Published online: 16 December 2025

References

1. Emma, P. et al. First lasing and operation of an ångstrom-wavelength free-electron laser. *Nat. Photonics*. **4**, 641–647 (2010).
2. Decking, W. et al. A MHz-repetition-rate hard X-ray free-electron laser driven by a superconducting linear accelerator. *Nat. Photonics*. **14**, 391–397 (2020).
3. Bergmann, U. et al. Using X-ray free-electron lasers for spectroscopy of molecular catalysts and metalloenzymes. *Nat. Rev. Phys*. **3**, 264–282 (2021).
4. Levantino, M. et al. Ultrafast myoglobin structural dynamics observed with an X-ray free-electron laser. *Nat. Commun.* **6**, 6772 (2015).
5. Hutchison, C. D. M., Perrett, S. & van Thor, J. J. XFEL beamline optical instrumentation for ultrafast science. *J. Phys. Chem. B*. **128**, 8855–8868 (2024).
6. Harmand, M. et al. Single-shot X-ray absorption spectroscopy at X-ray free-electron lasers. *Sci. Rep.* **13**, 18203 (2023).
7. Lemke, H. T. et al. Femtosecond X-ray absorption spectroscopy at a hard X-ray free electron laser: application to spin crossover dynamics. *J. Phys. Chem. A*. **117**, 735–740 (2013).
8. Bressler, C. et al. Femtosecond XANES study of the light-induced spin crossover dynamics in an iron(II) complex. *Science* **323**, 489–492 (2009).
9. Kim, Y. et al. Ligand-field effects in a ruthenium(II) polypyridyl complex probed by femtosecond X-ray absorption spectroscopy. *J. Phys. Chem. Lett.* **12**, 12165–12172 (2021).
10. Ochmann, M. et al. UV photochemistry of the L-cystine disulfide Bridge in aqueous solution investigated by femtosecond X-ray absorption spectroscopy. *Nat. Commun.* **15**, 8838 (2024).
11. Kondratenko, A. M. & Saldin, E. L. Generation of coherent radiation by a relativistic electron beam in an ondulator. *Part. Accel*. **10**, 207–216 (1980).
12. Bonifacio, R., Pellegrini, C. & Narducci, L. M. Collective instabilities and high-gain regime in a free electron laser. *Opt. Commun.* **50**, 373–378 (1984).
13. Gorobtsov, O. et al. Statistical properties of a free-electron laser revealed by Hanbury Brown-Twiss interferometry. *Phys. Rev. A*. **95**, 023843 (2017).
14. Gorobtsov, O. et al. Diffraction based Hanbury brown and Twiss interferometry performed at a hard x-ray free-electron laser. *Sci. Rep.* **8**, 2219 (2018).
15. Kim, Y. et al. Development of an experimental apparatus to observe ultrafast phenomena by tender X-ray absorption spectroscopy at PAL-XFEL. *J. Synchrotron Radiat.* **29**, 194–201 (2022).
16. Juranić, P. et al. Transient X-ray absorption near edge structure spectroscopy using broadband free-electron laser pulses. *Small Methods*. **8**, 2301328 (2024).
17. Inubushi, Y. et al. Spatially resolved single-shot absorption spectroscopy with x-ray free electron laser pulse. *Rev. Sci. Instrum.* **92**, 053534 (2021).
18. Min, C. K. et al. Hard X-ray self-seeding commissioning at PAL-XFEL. *J. Synchrot Radiat.* **26**, 1101–1109 (2019).
19. Nam, I. et al. High-brightness self-seeded X-ray free-electron laser covering the 3.5 keV to 14.6 keV range. *Nat. Photonics*. **15**, 435–441 (2021).
20. Amann, J. et al. Demonstration of self-seeding in a hard-X-ray free-electron laser. *Nat. Photonics*. **6**, 693–698 (2012).
21. Liu, S. et al. Cascaded hard X-ray self-seeded free-electron laser at megahertz repetition rate. *Nat. Photonics*. **17**, 984–991 (2023).
22. Kroll, T. et al. X-ray absorption spectroscopy using a self-seeded soft X-ray free-electron laser. *Opt. Express*. **24**, 22469–22480 (2016).
23. Eom, I. et al. Recent progress of the PAL-XFEL. *Appl. Sci.* **12**, 1010 (2022).
24. Choi, T. K. et al. Resonant X-ray emission spectroscopy using self-seeded hard X-ray pulses at PAL-XFEL. *J. Synchrot Radiat.* **30**, 1038–1047 (2023).
25. Kim, S. et al. Hard X-ray single-shot spectrometer of PAL-XFEL. *J. Synchrotron Radiat.* **32**, 246–253 (2025).
26. Kabanova, V. et al. Structure and spin of the low-and high-spin States of $Fe^{2+}(phen)_3$ studied by x-ray scattering and emission spectroscopy. *Struct. Dyn.* **11**, 054901 (2024).
27. Sato, T. et al. Capturing molecular structural dynamics by 100 Ps time-resolved X-ray absorption spectroscopy. *J. Synchrotron Radiat.* **16**, 110–115 (2009).
28. Katayama, T. et al. A versatile experimental system for tracking ultrafast chemical reactions with X-ray free-electron lasers. *Struct. Dyn.* **6**, 054302 (2019).

Acknowledgements

The experiments were performed using the XSS-FXL beamline at PAL-XFEL (Proposal No. 2022-1st-XSS-055) funded by the Ministry of Science and ICT of Korea.

Author contributions

R.R.M. and J.H.L. conceived the project and designed the experiments. R.R.M., J.H.L., I.N., G.K., G.P., and M.S.K. prepared and performed the TR-XAS experiments with self-seeded FEL. R.R.M., Y.J.K and J.H.L analyzed the data and prepared figures. R.R.M., Y.J.K and J.H.L wrote the manuscript with input from all authors. All authors discussed the results and contributed to the final manuscript.

Funding
This research was supported by Basic Science Research Program through the National Research Foundation of Korea(NRF) funded by the Ministry of Education(Grant number_2022R1I1A1A01062991, 2022M3H4A1A04074153).

Declarations

Competing interests
The authors declare no competing interests.

Additional information
Correspondence and requests for materials should be addressed to J.H.L.

Reprints and permissions information is available at www.nature.com/reprints.

Publisher's note Springer Nature remains neutral with regard to jurisdictional claims in published maps and institutional affiliations.